property of composite scaffold for different strand orientations. Compressive strength and compressive modulus properties of the samples were found using Instron 4467 mechanical tester with a load cell of 30 kN. In order to smoothen the contact surface for compression, samples were slightly filed before testing. The load was applied at normal room temperature conditions with no preloading at a crosshead velocity of 1mm/min [Serra, Planell and Navarro (2013); Ramay and Zhang (2004)].

2.5 Fourier transform infrared spectroscopy (FTIR)

To find the components of scaffold samples, Fourier transform infrared spectroscopy was performed. Nicolet is5 ranging from 4000/cm to 400/cm from Thermo Scientific (Waltham, MA, USA) was used to record infrared absorbance spectra of sintered β-TCP/Zirconia scaffolds. To get the final plot, a spectrum of atmospheric moisture was taken out without the sample and was further subtracted from the actual sample spectra as an open system of measurement was used [Sarikaya and Aydin (2015)].

2.6 Scanning electron microscopy (SEM)

Scanning electron microscope was used to analyze the macro pore distribution, strand size and distance between adjacent strands in manufactured β-TCP/Zirconia scaffolds after sintering. The double adhesive tape was used to place the samples on aluminum studs and JEOL JFC 1600 Auto fine coater from Japan was used to coat the samples with gold-palladium. Pictures at different magnifications were taken using JOEL-6380A scanning electron microscope [Haberstroh, Ritter and Kuschnierz et al. (2010)].

2.7 X-ray diffraction analysis (XRD)

X-ray diffractometer (XRD) examined the crystalline phases of TCP/Zirconia scaffolds. X'Pert PRO, PANalytical scanned the samples from 10^o – 70^o (2θ) where θ is the diffraction angle, at a scan rate of 1^o 2θ min^{-1}. The samples rested on aluminum supports using double adhesive tape and the copper tube was operated at 45 kV and 40 mA.

2.8 Cell culture and cytotoxicity assay

2.8.1 Materials

National Centre for Cell Science (NCCS) (Pune, Maharashtra, India) helped us in acquiring human Osteosarcoma cell line (MG-63 cell line). Himedia, India provided us with heat-inactivated fetal bovine serum, antibiotic solution, phosphate buffered saline and Dulbecco's modified eagle medium (DMEM). N-methyl sulfate (PMS), 2,3-bis-[2-methoxy-4-nitro-5sulfophenyl]-2H-tetrazolium-6-caroxanilide inner salt (XTT), and other chemicals were procured from Sigma Co. (St. Louis, MO, USA). Axiva Sichem Pvt. Ltd. (New Delhi, India) provided plastic wares used for cell culture.

2.8.2 Culture of MG-63 cells

DMEM medium was supplemented with 10 µl/ml penicillin, 10% heat-inactivated fetal bovine serum, 25 µg/ml streptomycin and 25 µg/ml amphotericin B (complete DMEM medium) to routinely maintain MG-63 cells. After every 4-5 days, cells were sub-cultured.

2.8.3 Trypsinization protocol for sub-culturing

PBS was used to wash confluent cells in order to remove excess medium. Further, 2 ml of 0.05% trypsin and (0.04%) 5 mM EDTA was added to the flask to trypsinize the cells. The flask was kept in the incubator for 2 to 3 min to bring the cells in the suspension form. The culture medium of the equal volume was added to the suspended free cells to stop trypsinization. 15 ml centrifuge tube was used to collect suspended cells and centrifugation was done at 1000 RPM for 10 min. The supernatant was discarded and fresh DMEM culture medium was used to re-suspend the cells after centrifugation. WBS counting chamber (Neuber's chamber) was used to count the cells as per standard protocol.

2.8.4 Cell cytotoxicity assay

XTT assay was used to evaluate in-vitro cell proliferation ability of each architecture type. XTT was used to assess cell proliferation after 18, 36 and 54 hours for human Osteosarcoma cells which were seeded in the presence and absence of scaffolds in a 24 well plate (4 × 104 cells/ml). 40 µl of XTT containing phenazine metrosulphate (PMS) (1 mg/ml XTT solution) was added to each sample and then kept in an incubator at 37° C in 5% CO2 humidified atmosphere for 4 hours. Robonic Readwell ELISA well plate analyzer was then used to measure the absorbance at 450 nm. In culture medium, 100% viability was considered for well-containing cells without scaffolds and the absorbance of these cells was used as a control for comparison.

3 Results and Discussion

3.1 Physical and mechanical analysis of scaffolds

Physical analysis demonstrated light-yellow shade to the scaffolds after sintering and also continuous interconnected compact structures were exposed by the scaffolds. Volumetric shrinkage was the only deformation due to high-temperature sintering. No other deformations like the geometry of the pores, variation in the architecture or breakage of the strands were observed. After sintering the scaffolds, 14 mm x 14 mm x 4.66 mm dimensions were obtained which measured 15 mm x15 mm x 5 mm before sintering. There are two main reasons for the shrinkage: First, diffusion of HA/TCP particles and second, evaporation of binder. Mechanical and porosity testing revealed higher strength and porosity values of 12.025 Mpa and 69.27% respectively for the scaffold with 0° - 72° -144° -36° -108° architecture. Scaffold with 0° - 108° -216° architecture though has highest porosity value but demonstrates low mechanical strength. Scaffolds with (0° - 90°) and (0° - 45° - 90°-135°) showed comparable values for strength and porosity. Further, in order to find the best architecture which has optimum mechanical strength, porosity and cell culture capability, all the samples were tested for its cell proliferation abilities.

Table 1: Mechanical results obtained for composite scaffolds sintered at 1500° C

Strand Orientation	Strand Size (μm)	Dist. b/w Strands (μm)	Total Porosity (*p*) (%)	Compressive Modulus (Mpa)	Compressive Strength (Mpa)
0° – 90°	400	1000	60.06	197.4383	9.403
0° – 45° – 90° – 135°	400	1000	66.56	226.456	11.785
0° – 108° – 216°	400	1000	76.46	160.398	7.639
0° - 72° - 144° - 36° - 108°	400	1000	69.27	204.199	12.025

3.2 FTIR & XRD analysis

To find the phases present in the sintered scaffolds, FTIR analysis was used to examine the functional groups after sintering in β-TCP / Zirconia scaffolds. Due to absorbed moisture, bands around 3426.18 cm^{-1} and 1633 cm^{-1} is visible and assigned to the stretching vibration of O-H bond. Absorption of non-bridging OH group is evident and is shown by the peaks around 1384cm^{-1}. Also, the monoclinic structure of ZrO_2 has been assigned the sharp bends around 745 cm^{-1} and the tetragonal structure of ZrO_2 has been assigned the wide bands of 550 cm^{-1} and 610 cm^{-1}. The presence of three single P-O bonds was indicated by bands from 1029.65 cm^{-1} to 1051.31cm^{-1} and that of the P-O single double bond was indicated by bands around 970 cm^{-1} in β-TCP. Different FTIR spectra showed no major variation. For all the samples, the presence of β-TCP, ZrO_2 along with $CaZrO_3$ peaks with 30% ZrO2 content was revealed by XRD profile of the sample sintered at 1500° C. $CaZrO_3$ was formed due to the reaction between ZrO_2 and CaO, where CaO is produced due to the decomposition of β-TCP at high temperature. When CaO gets dissolved in ZrO_2, the Cubic phase of ZrO_2 is formed from the tetragonal phase. Among the different samples, no major variations were observed in XRD profile.

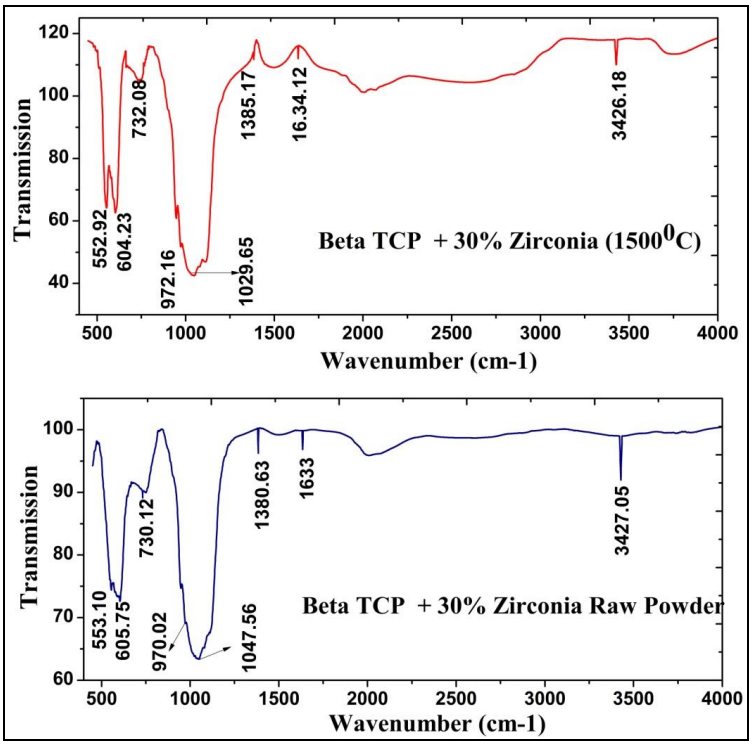

Figure 3: FTIR profile for β-TCP/Zirconia scaffold sintered at 1500° C

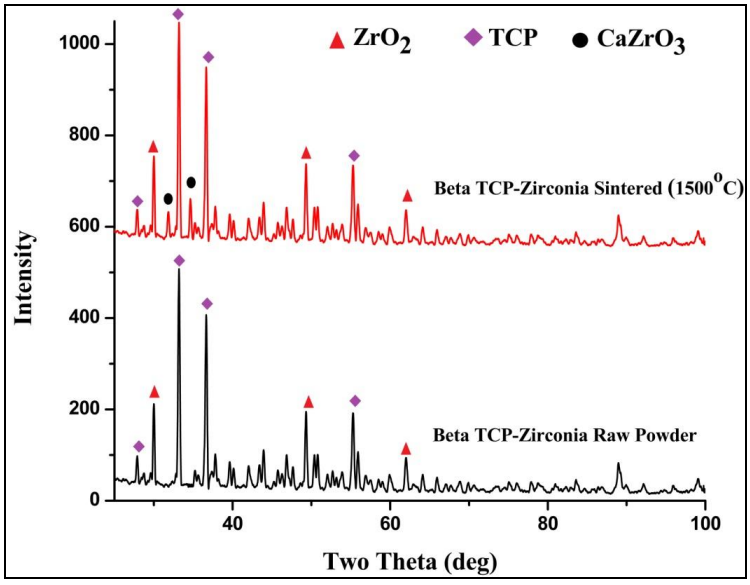

Figure 4: XRD pattern for β-TCP/Zirconia scaffold sintered at 1500° C

3.3 Scanning electron microscopy analysis

Uneven distribution of macro porosity is caused due to powder material processing. For efficient transport of nutrients and oxygen, macropores ranging from 666 µm to 705 µm are present in all samples and is shown by SEM micrograph. Also, on the scaffold surface, micropores were observed (3 to 32 µm) which is required for the initial cell adhesion. For efficient cell growth and nutrient transport, high level of interconnected porosity is required as stated previously in the text. It was observed that the overall porosity and pore connectivity network of the scaffold was affected with the type of architecture and reduction in the proportional volume of the sample was also observed. Removal of water vapor and binder from the scaffold surface and conversion of tetragonal to the cubic structure of ZrO_2 are the reasons that may be attributed to the decrease in porosity of the scaffold samples. Conversely, an increase in compressive strength was observed for sample with staggered architecture. Sample with (0^o - 72^o - 144^o - 36^o - 108^o) structure exposed more strength and porosity value, this may be attributed to the increase in the micro porosity associated with it. Without any perceptible distortion, the surface of the scaffolds maintained their respective structure after sintering.

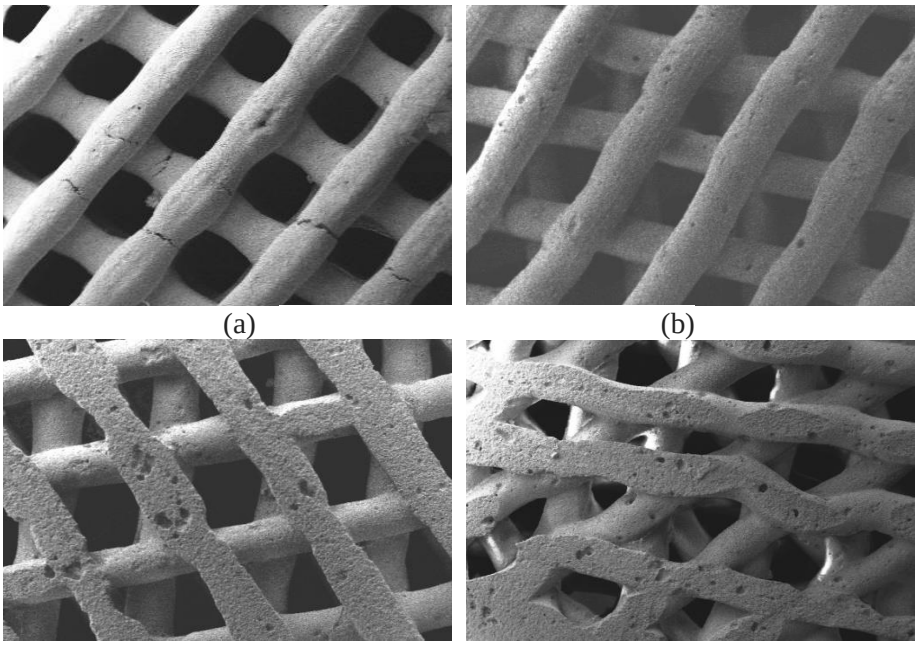

Figure 5: SEM micrograph of HA/TCP/Collagen scaffolds with different lay down pattern (a) 0^o - 90^o (b) 0^o - 72^o - 144^o - 36^o - 108^o (c) 0^o - 108^o - 216^o (d) 0^o - 45^o - 90^o - 135^o.

3.4 Cell cytotoxicity

XTT assay was performed to evaluate cell proliferation of β-TCP/Zirconia composite scaffold for 18, 36 and 54 hours. For scaffolds with 0^o -90^o, 0^o - 45^o - 90^o -135^o and 0^o -

72º - 144º - 36º - 108º architecture, there was an increase in optical density values with culture time. On the other hand, optical density values for the scaffold with 0º -108º-216º decreased. Further after 54 hours of incubation scaffold with 0º - 72º - 144º - 36º - 108º structure displayed the maximum OD value. This proves that scaffold with 0º-72º - 144º - 36º - 108º structure has morphologically well spread inside architecture which further helps cells to perfectly adhere, migrate and proliferate.

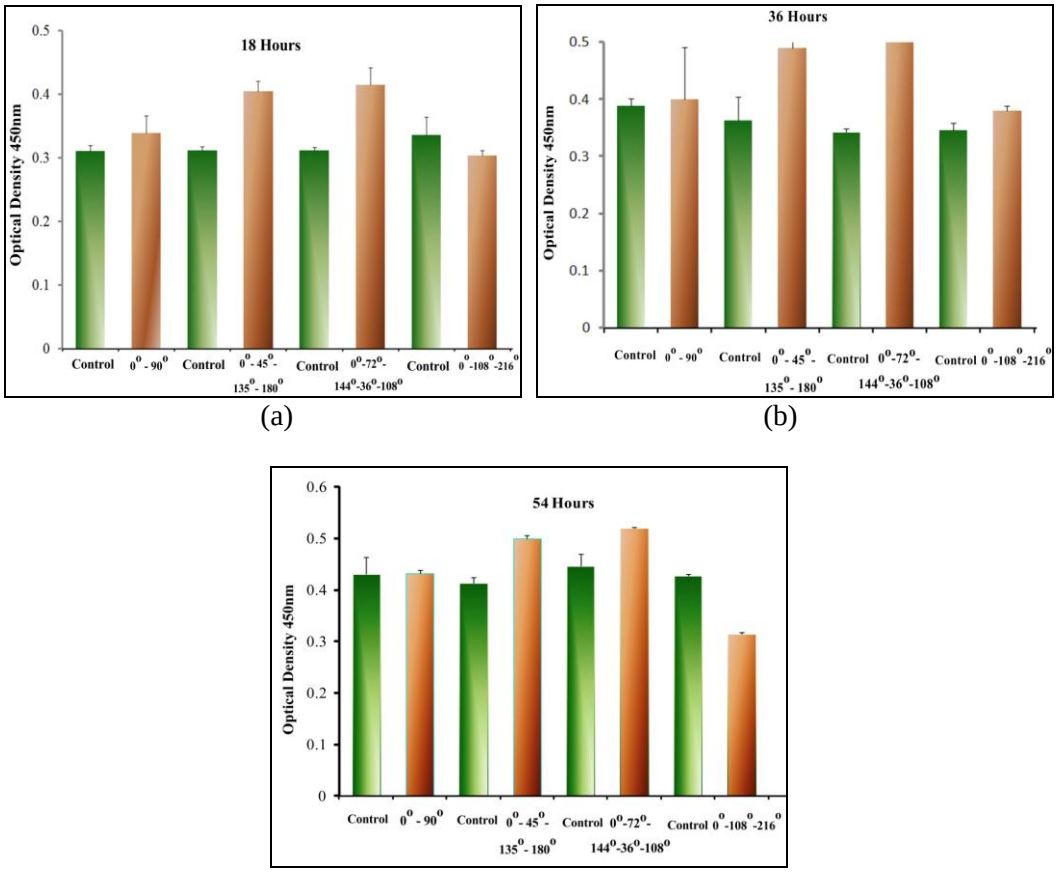

Figure 6: The depiction of optical density values for β-TCP/Zirconia scaffolds sintered at 1500º C for 18 h (a), 36 h (b) and 54 (c).

4 Conclusion

In the present study, Beta TCP-Zirconia composite scaffolds were fabricated using the 3D-Bioplotting system. Four different architectures were fabricated and were further evaluated for its mechanical strength and Cell proliferation capabilities. After high-temperature sintering, it was revealed that scaffold with 0º-72º-144º-36º-108º architecture presented excellent mechanical and cell proliferation ability. It is concluded that the present architecture with 70/30 Beta TCP-Zirconia ratio is very promising for application where bone grafting is essential to heal large size Bone defects. Future studies will include

fabrication of Haversian canals inside the scaffold architecture in order to facilitate the formation of blood vessels and promote vascularization.

5 Future Scope

Future studies will include the development of a computer programme for the fabrication of patient-specific scaffold directly from the CT data of the patient. The CT data collected in DICOM format can be used to find the point cloud to get the 3D volumetric model of the defective part. Further, the model can be saved in. STL file format which can be directly uploaded to the 3D printing machine. Also, computed assisted modeling of different scaffold architectures in relation to their mechanical strength, interconnectivity, porosity and pore size will be addressed in future studies. Furthermore, a computer programme for modeling of Volkmann's canals and Haversian canals which are responsible for efficient nutrients transport will be part of future studies.

Conflict of interest statement: The authors declare no conflict of interest.

References

Gao, C.; Deng, Y.;Feng, P.; Mao, Z.; Li, P.; Yang, B.; Deng, J.;Cao, Y.; Shuai, C.P.S. (2014): Current progress in bioactive ceramic scaffolds for bone repair and regeneration. *Int. J. Mol Sci*, vol.15, pp.4714-4732.

Guan, J.; Fujimoto, K.L.; Sacks, M.S.W.W. (2005): Preparation and characterization of highly porous, biodegradable polyurethane scaffolds for soft tissue applications. *Biomaterials*, vol.26, pp.3961-3971.

Haberstroh, K.; Ritter, K.; Kuschnierz, J., et al (2010): Bone repair by cell-seeded 3D-bioplotted composite scaffolds made of collagen treated tricalciumphosphate or tricalciumphosphate-chitosan-collagen hydrogel or PLGA in ovine critical-sized calvarial defects. *J. Biomed Mater Res-Part B Appl Biomater*, vol.93, pp.520–530, doi: 10.1002/jbm.b.31611.

Jariwala, S.H.; Lewis, G.S.; Bushman, Z.J., et al (2015): 3D Printing of Personalized Artificial Bone Scaffolds. *3D Print Addit Manuf*, vol.2, pp.56-64, doi: 10.1089/3dp.2015.0001.

Mohamed, K.R.; Mohamed, A.M.; Beherei, H.H. (2011): Synthesis and in vitro behavior of β-TCP zirconia/polymeric biocomposites for bio-applications. *J. Genet Eng Biotechnol, vol.* 9, pp.111-119, doi: 10.1016/j.jgeb.2011.09.001.

Mohamad Yunos, D.; Bretcanu, O.; Boccaccini, A.R. (2008): Polymer-bioceramic composites for tissue engineering scaffolds. *J. Mater Sci.*, vol.43, pp.4433, doi: 10.1007/s10853-008-2552-y.

Ramay, H.R.R.; Zhang, M. (2004): Biphasic calcium phosphate nanocomposite porous scaffolds for load-bearing bone tissue engineering. *Biomaterials*, vol.25, pp.5171-5180, doi: 10.1016/j.biomaterials.2003.12.023.

Rapacz-Kmita, A.; Ślósarczyk, A; Paszkiewicz, Z. (2006): Mechanical properties of Hap-ZrO2 composites. *J. Eur Ceram Soc, vol.*26, pp.1481-1488, doi: https://doi.org/10.1016/j.jeurceramsoc.2005.01.059.

Sarkar, S.K.; Lee, B.T. (2015): Hard tissue regeneration using bone substitutes: an update on innovations in materials. *Korean J. Intern Med*, 30:279-293, doi: 10.3904/kjim.2015.30.3.279.

Sapkal, P.S.; Kuthe, A.M.; Kashyap, R.S., et al (2016): Rapid prototyping assisted fabrication

of patient specific β-tricalciumphosphate scaffolds for bone tissue regeneration. *J. Porous Mater*, vol.23, pp.927-935, doi: 10.1007/s10934-016-0150-y.

Sapkal, P.S.; Jaiswal, S.; M. Kuthe, A. (2016): Rapid Prototyping Assisted Scaffold Fabrication for Bone Tissue Regeneration. *J. Mater Sci Res*, vol.5, pp.79, doi: 10.5539/jmsr.v5n4p79.

Sapkal, P.S.; Kuthe, A.M.; Kashyap, R.S., et al (2016): Indirect fabrication of hydroxyapatite/β-tricalcium phosphate scaffold for osseous tissue formation using additive manufacturing technology. *J. Porous Mater, vol.*23, pp.1567-1574, doi: 10.1007/s10934-016-0217-9.

Sapkal. P.S. (2016): CAD Based Approach for Patient Specific Scaffold for Bone Tissue Engineering.Original Article CAD Based Approach for Patient Specific Scaffold for Bone Tissue Engineering, vol.29, pp.301-305.

Sapkal, P.S.; Kuthe, A.M.; Kashyap, R.S., et al (2017): Indirect casting of patient-specific tricalcium phosphate zirconia scaffolds for bone tissue regeneration using rapid prototyping methodology. *J. Porous Mater*, vol.24, pp.1013-1023, doi: 10.1007/s10934-016-0341-6.

SUN, A.; MENG, Q.; LI, W., et al (2015): Construction of tissue-engineered laryngeal cartilage with a hollow, semi-flared shape using poly (3-hydroxybutyrate-co-3-hydroxyhexanoate) as a scaffold. *Exp Ther Med, vol.* 9, pp.1482-1488 , doi: 10.3892/etm.2015.2262.

Serra, T.; Planell, J. A.; Navarro, M. (2013): High-resolution PLA-based composite scaffolds via 3-D printing technology. *Acta Biomater*, vol.9, pp.5521-5530, doi: 10.1016/j.actbio.2012.10.041

Sarikaya, B.; Aydin, H. M. (2015): Collagen/Beta-Tricalcium Phosphate Based Synthetic Bone Grafts via Dehydrothermal Processing. *BioMed Research International*, vol.2015,doi: 10.1155/2015/576532.

Wang, M. (2007) : *Materials Selection and Scaffold Fabrication for Tissue Engineering in Orthopaedics BT-Advanced Bioimaging Technologies in Assessment of the Quality of Bone and Scaffold Materials: Techniques and Applications*. In: Qin L, Genant HK, Griffith JF, Leung KS (eds). Springer Berlin Heidelberg, Berlin, Heidelberg, pp. 259-288.

Wang, Q.; Wang, Q.; Wan, C. (2011): the Effect of Porosity on the Structure and Properties of Calcium Polyphosphate Bioceramics. *Ceram-Silikáty*, vol.55, pp.43-48.

Xiong, Z. (2002): Fabrication of porous scaffolds for bone tissue engineering via low-temperature deposition. *Scr Mater, vol.*46, pp.771-776, doi: 10.1016/S1359-6462(02)00071-4.